Extrapolation of Electromagnetic Responses from Conducting Objects in Time and Frequency Domains

Murli Mohan Rao, Tapan Kumar Sarkar, *Fellow, IEEE,* Raviraj S. Adve, Tricha Anjali, and Jesús Fornieles Callejón

***Abstract*— Utilizing early time response and low-frequency data, the complete electromagnetic response of a three-dimensional conducting structure is generated. By using mutually complementary data, simultaneous extrapolation in time and frequency domains are carried out. This is performed through the use of the associated Hermite polynomials. The interesting property of the Hermite polynomials is that they are the eigenfunctions of the Fourier transform operator. This implies that if the time-domain response at a point in space from a three-dimensional conducting object is modeled by an associated Hermite series expansion, the frequency-domain response at the same point can be expressed as a scaled version of the same time-domain representation. Therefore using early time and low-frequency-domain response data, it is possible to reproduce the missing response in both of the domains. Examples are presented to illustrate the application of this methodology.**

***Index Terms*—Broad-band, electromagnetic scattering, extrapolation, Hermite polynomials.**

I. Introduction

IN TRADITIONAL computational electromagnetics, analysis is carried out exclusively in either the time or frequency domains. Some of the popular methods for performing the analysis in the time domain are, e.g., the finite-difference, finite-element, or integral-equation approaches. The objective here is to solve either the integral or differential form of Maxwell's equations solely in the time domain. The way to analyze electrically large problems is to use a bigger and faster computer. In addition, analytical continuation method can be used to extrapolate the time-domain data. For example, the matrix pencil technique [1] can be utilized to extrapolate late time response from conducting objects. However, in practice, it is difficult to discriminate between the early and late time response from an object, e.g., particularly if the structure is an elongated cavity. In this case, due to multiple bounces of the electromagnetic response inside the cavity, it is difficult to predict what is the late time response.

In the frequency domain, one essentially employs the same way of thinking. The Maxwell's equations are solved entirely in the frequency domain utilizing either the finite-difference, finite-element, or integral-equation approach. Unlike in the time domain, here one needs to solve a matrix equation that becomes large as the electrical dimension of the structure increases. The methodology to perform electromagnetic analysis of a large complex structure is to use a super computer as one needs to solve a large matrix equation at each frequency point of interest. Even though extrapolation techniques [2] have been developed utilizing the Cauchy method, one may still be performing data extrapolation to generate a wide-band response.

Extrapolation in either the time or frequency domains is sometimes a numerically unstable process, and its accuracy often cannot be guaranteed. Hence, the desire to perform accurate extrapolation in either the time or frequency domains leads to the idea of simultaneous extrapolation in the time and frequency domains. In this methodology, the goal is not so much on extrapolation of data, but how to generate the missing data. The use of early time response and low-frequency information provides all the information that is required, but it is in the mutually complementary domain. The low frequency provides the late time information, whereas the early time provides the high-frequency information. Therefore, by using such a hybrid methodology, one is not creating new information by performing extrapolation carried out exclusively in one domain, but simply extracting the information that already exists in the mutually complementary data sets.

In this paper, the hybrid technique utilizing early time and low-frequency information is used to generate the information for all time and frequency. Hence, one uses a time-domain code and generates the early time information. Next, one uses a frequency-domain code and generates the low-frequency information. The generation of this information is quite simple and not very computation intensive. Next, the associate Hermite (AH) polynomials are used to extrapolate the information simultaneously in both domains. This is in contrast to the fast-Fourier-transform-based techniques presented earlier [3] or by using the Hilbert transform [4].

Manuscript received March 27, 1998. This work was supported in part by the Office of Naval Research under Contract N00014-98-1-0279, and in part by E. I. Dupont de Nemours and Company.

M. M. Rao is with rlemedia, Bell Laboratories, Lucent Technologies, Holmdel, NJ 07733 USA.

T. K. Sarkar, R. S. Adve, and T. Anjali are with the Department of Electrical and Computer Engineering, Syracuse University, Syracuse, NY 13244-1240 USA.

J. F. Callejón is with the Department Fisica Applicada, Universidad de Granada, Granada, Spain.

Publisher Item Identifier S 0018-9480(99)07704-2.

II. AH Polynomials

The AH polynomials $h_n(t)$ are defined in terms of the Hermite polynomials $H_n(t)$. They are

$$h_n(t) = \frac{H_n(t)e^{(-t^2/2)}}{(2^n n!\sqrt{\pi})^{1/2}}. \tag{1}$$

The Hermite polynomials are generated recursively through

$$\begin{aligned} H_o(t) &= 1 \\ H_1(t) &= 2t \\ H_n(t) &= 2tH_{n-1}(t) - 2(n-1)H_{n-2}(t), \qquad \text{for} \quad n \geq 2. \end{aligned} \tag{2}$$

The AH functions are, therefore, computed from

$$\begin{aligned} h_o(t) &= \frac{e^{-(t^2/2)}}{(\sqrt{\pi})^{1/2}} \\ h_1(t) &= \frac{2te^{-(t^2/2)}}{(2\sqrt{\pi})^{1/2}} \end{aligned} \tag{3}$$

and

$$\begin{aligned} &h_n(t) \\ &= \frac{1}{\sqrt{n}}\left[\sqrt{2}\,t h_{n-1}(t) - \sqrt{n-1}\,h_{n-2}(t)\right], \qquad \text{for} \quad n \geq 2. \end{aligned}$$

In addition, the AH polynomials are orthogonal to each other and form a complete set in the interval $[-\infty, \infty]$ as

$$\int_{-\infty}^{\infty} h_i(t)h_j(t)\,dt = \delta_{ij} \tag{4}$$

where the delta function is defined by

$$\left.\begin{aligned} \delta_{ij} &= 1, \qquad \text{for } i = j \\ &= 0, \qquad \text{otherwise} \end{aligned}\right\}. \tag{5}$$

In addition, the AH polynomials of even order are even, and of odd orders are odd, i.e.,

$$\left.\begin{aligned} h_{2k}(t) &= h_{2k}(-t) \\ h_{2k+1}(t) &= -h_{2k+1}(-t) \end{aligned}\right\} \tag{6}$$

for any value of k. Therefore, it follows that

$$\left.\begin{aligned} h_{2k+1}(0) &= 0 \\ h_{2k}(0) &= \sqrt{\frac{1}{\pi}\frac{\Gamma(k+0.5)}{\Gamma(k+1)}} \end{aligned}\right\} \tag{7}$$

where the gamma function $\Gamma(k)$ is defined through

$$\left.\begin{aligned} \Gamma(t) &= (t-1)\Gamma(t-1) \\ \Gamma(-t) &= -t\Gamma(t-1), \qquad \text{with} \quad t \neq 0, 1, 2, 3 \cdots \\ \Gamma(1) &= 1 \\ \Gamma(0.5) &= \sqrt{\pi}. \end{aligned}\right\} \tag{8}$$

Therefore, if $y(t)$ is a piecewise smooth function in every finite interval $[-p, p]$ and

$$\int_{-\infty}^{\infty} e^{-t^2}\, y^2(t)\,dt < \infty \tag{9}$$

then the AH series

$$y(t) = \sum_{n=o}^{\infty} a_n h_n(t), \qquad \text{for } -\infty < t < \infty \tag{10}$$

with

$$a_n = \int_{-\infty}^{\infty} y(t)h_n(t)\,dt \tag{11}$$

converges pointwise to $y(t)$ at every continuity point and converges to $[y(t^+) + y(t^-)]/2$ at the points of discontinuity.

In addition, the AH functions are eigenfunctions of the Fourier transform operator. If we define $\tilde{h}_n(f)$ to be the Fourier transform of $h_n(t)$, then with $j = \sqrt{-1}$

$$\tilde{h}_n(f) = \int_{-\infty}^{\infty} h_n(t)\,\exp(-j2\pi ft)\,dt = (-j)^n h_n(f). \tag{12}$$

Therefore, if we consider $Y(f)$ to be the Fourier transform of $y(t)$, then it appears

$$\begin{aligned} Y(f) &= \int_{-\infty}^{\infty} y(t)\,\exp(-j2\pi ft)\,dt \\ &= \int_{-\infty}^{\infty} \sum_n a_n h_n(t)\,\exp(-j2\pi ft)\,dt \\ &= \sum_n a_n(-j)^n h_n(f). \end{aligned} \tag{13}$$

The existence of (10) and (13) indicates that the same functions $h_n(t)$ cannot only be used to approximate the time-domain functions, but a scaled version of it can be simultaneously used to represent its transform. Therefore, we can use the same functional representation to approximate the time-domain and the frequency-domain electromagnetic responses. However, for ease of manipulations, we will be using a slightly modified versions of (10) and (13).

III. The Mathematical Formulation

Let $x(t)$ represent the electromagnetic response at a spatial location due to an applied stimulus $s(t)$. We then have

$$x(t) = \sum_{n=o}^{N} \frac{a_n}{\sqrt{q_1}}\, h_n(t/q_1) \tag{14}$$

where q_1 is a scale factor that scales the time variable. In practice, the summation in (10) cannot go to infinity and, therefore, for practical computational reasons, it is only up to some value N. Thus, we are basically representing the early time response at a point in space by (14).

Next, we consider the frequency-domain response. By virtue of (13), one can write

$$\begin{aligned} X(f) &= \int_{-\infty}^{\infty} x(t)\,\exp(-j2\pi ft)\,dt \\ &= \sum_{n=o}^{N} (-j)^n \frac{a_n}{\sqrt{q_2}}\, h_n(f/q_2) \\ &= \sum_{n=o}^{N/2} (-1)^n \left[\frac{a_{2n}}{\sqrt{q_2}}\, h_{2n}(f/q_2) - j\frac{a_{2n+1}}{\sqrt{q_2}}\, h_{2n+1}(f/q_2)\right] \\ &= X_R(f) + jX_I(f). \end{aligned} \tag{15}$$

Here, q_2 is the scale factor in dealing with the frequency variable. The quantities q_1 and q_2 have been introduced to make the computation of the AH functions within a certain interval for stable numerical computation.

A word of caution: since time-domain signals in real life are causal, i.e.,

$$x(t) = 0, \qquad \text{for} \quad t < 0 \tag{16}$$

it is necessary to approximate not $x(t)$ in (14), but $x(t + t_o)$. Here, we prefer to center the expansion of the Hermite polynomials not at $t = 0$, but rather at $t = t_o$, where t_o is roughly around half the time support of $x(t)$. This is because the AH functions provide equal support on either side of the center of the expansion. Thus, centering the expansion about t_o would require fewer terms in the expansion. Therefore, we now work with the transform pair $x(t + t_o) \leftrightarrow X(f) \cdot \exp(j2\pi f t_o)$.

The choice of the scaling factor q_1 is crucial because it also affects q_2. Also, q_1 and q_2 decide the amount of support given by the AH functions to the time- and frequency-domain responses, respectively. Given about 50%–60% of initial time-domain data and an equal amount of low-frequency data, with a proper choice of N, the order of the expansion, and q_1, the scaling factor, it is possible to extrapolate in both domains.

In all the examples, a choice of q_1 is made such that the t- and f-axes are roughly scaled to the same range. The order of expansion (N) is obtained by first using a large value, then, depending on a threshold criterion, the expansion is truncated. The value of N can be decided by choosing a cutoff for the magnitude of the coefficients, i.e., discarding the ones that die out. More specifically, in all the examples presented, the expansion was truncated if three consecutive coefficients were less than 0.5% of the largest coefficient. Choosing an unnecessarily large N will introduce oscillations in the extrapolation region. The coefficients are obtained by solving a least-squares problem, using singular value decomposition (SVD) [8].

Let M_1 and M_2 be the number of time- and frequency-domain samples that are given. The matrix representation of time-domain data, from (10), would then be

$$\begin{bmatrix} h_0(t_1/q_1) & h_1(t_1/q_1) & \cdots & h_{N-1}(t_1/q_1) \\ h_0(t_2/q_1) & h_1(t_2/q_1) & \cdots & h_{N-1}(t_2/q_1) \\ \vdots & \vdots & \vdots & \vdots \\ h_o(t_{M_1}/q_1) & h_1(t_{M_1}/q_1) & \cdots & h_{N-1}(t_{M_1}/q_1) \end{bmatrix}_{M_1 \times N} \cdot \begin{bmatrix} a_0 \\ a_1 \\ \vdots \\ a_{N-1} \end{bmatrix}_{N \times 1} = \sqrt{q_1} \begin{bmatrix} x(t_1) \\ x(t_2) \\ \vdots \\ x(t_{M_1}) \end{bmatrix}_{M_1 \times 1}. \tag{17}$$

The real part of $X(f)$, from (15), can be represented by the even-order functions, as shown in (18), at the bottom of this page. The imaginary part of $X(f)$, from (15), can be represented, by the odd-order functions, as shown in (19), at the bottom of this page. Combining the three matrix equations, we get (20), shown at the bottom of the following page. The coefficients of the expansion are obtained by solving this matrix equation.

IV. Numerical Examples

In this section, six examples are presented to validate the above technique. A program to evaluate the currents on an arbitrarily shaped closed or open body using the electric-field integral equation (EFIE) and triangular patching is used [5]. The rationale for doing this is that we are going to use the EFIE both in time [6] and frequency domain [5]. We utilize the same surface patching scheme for both domains; hence, eliminating some of the effects of discretization from this study. The triangular patching approximates the surface of the scatterer with a set of adjacent triangles. The current perpendicular to each nonboundary edge is an unknown to be solved for. The frequency-domain data was generated using the program described in [5]. However, in the last example, of the cone hemisphere, the magnetic-field integral equation (MFIE) is preferred due to the instability of the EFIE formulation [7]. Quadrilateral patching is used with the MFIE approach.

Although the program can be used with an arbitrary excitation, we used a linearly polarized plane wave with a Gaussian

$$\begin{bmatrix} h_0(f_1/q_1) & -h_2(f_1/q_2) & \cdots & (-1)^{N/2-1} h_{N-1}(f_1/q_2) \\ h_0(f_2/q_2) & -h_2(f_2/q_2) & \cdots & (-1)^{N/2-1} h_{N-1}(f_2/q_2) \\ \vdots & \vdots & \vdots & \vdots \\ h_o(f_{M_2}/q_2) & -h_2(f_{M_2}/q_2) & \cdots & (-1)^{N/2-1} h_{N-1}(f_{M_2}/q_2) \end{bmatrix}_{M_2 \times N/2} \begin{bmatrix} a_0 \\ a_2 \\ \vdots \\ a_{N-2} \end{bmatrix}_{N/2 \times 1} = \sqrt{q_2} \begin{bmatrix} X_R(f_1) \\ X_R(f_2) \\ \vdots \\ X_R(f_{M_1}) \end{bmatrix}_{M_2 \times 1} \tag{18}$$

$$\begin{bmatrix} -h_1(f_1/q_1) & h_3(f_1/q_2) & \cdots & (-1)^{N/2} h_{N-2}(f_1/q_2) \\ -h_1(f_2/q_2) & h_3(f_2/q_2) & \cdots & (-1)^{N/2} h_{N-2}(f_2/q_2) \\ \vdots & \vdots & \vdots & \vdots \\ -h_1(f_{M_2}/q_2) & h_3(f_{M_2}/q_2) & \cdots & (-1)^{N/2} h_{N-2}(f_{M_2}/q_2) \end{bmatrix}_{M_2 \times N/2} \begin{bmatrix} a_1 \\ a_3 \\ \vdots \\ a_{N-1} \end{bmatrix}_{N/2 \times 1} = \sqrt{q_2} \begin{bmatrix} X_1(f_1) \\ X_1(f_2) \\ \vdots \\ X_1(f_{M_2}) \end{bmatrix}_{M_2 \times 1} \tag{19}$$

profile in time. The excitation has the form

$$\mathbf{E}^{\text{inc}} = \mathbf{u_i} \frac{E_o}{\sigma c \sqrt{\pi}} e^{-\gamma^2} \tag{21}$$

where,

$$\gamma = \frac{(t - t_o - \mathbf{r} \cdot \mathbf{k})}{\sigma} \tag{22}$$

- u_i unit vector that defines the polarization of the incoming plane wave;
- E_o amplitude of the incoming wave;
- σ controls the width of the pulse;
- t_o a delay and is used so the pulse rises smoothly from zero for time $t < 0$ to its value at time t;
- r position of an arbitrary point in space;
- k unit wave vector defining the direction of arrival of the incident pulse.

To find the frequency response to the above Gaussian plane wave, the transfer function of the system is multiplied by the spectrum of the incident Gaussian plane wave. The input spectrum is given by

$$G(\omega) = \frac{E_o}{c} e^{-[(\pi\sigma f)^2 + j\omega t_o]}, \qquad \omega = 2\pi f. \tag{23}$$

The time and frequency domain form of the incident wave is shown in Fig. 1 for Example 1.

In all our computations, E_o is chosen to be 377 V/m. The time step (Δt) is dictated by the discretization used in modeling the geometry of each example. The frequency step (Δf) is either 1 or 2 MHz depending on the problem.

In all examples, the extrapolated time-domain response is compared to the output of the marching-on-in-time (MOT) program [6]. Also, the extrapolated frequency-domain response modified by the spectrum of the incident wave is compared to the frequency response obtained from the method-of-moments (MoM) program [5]. In all the plots, extrapolated signal refers to the extrapolated response using AH expansions while original signal refers to the data obtained from the MOT or MoM program.

A. Example 1—Unequal Plates

In this example, we have two square plates of zero thickness and sides 1 and 2 m in the xy-plane. The configuration with the discretization is shown in Fig. 2. The separation between the plate is 1 m. The excitation arrives from the direction $\theta = 0$, $\phi = 0$; i.e., along the negative z-direction, u_i is along the x-axis. The time step used in the MOT program is 196.8 ps. In this example, $\sigma = 0.79$ ns and $t_o = 9.20$ ns. The edge under consideration is on the smaller plate, in the y–direction and center. On that edge, we would like to generate the information about the current for all times and frequencies for the given excitation from the information of the current for early times and low frequencies.

Using the MOT algorithm, time-domain data is obtained from $t = 0$ to $t = 50$ ns (250 data points). Also, frequency-domain data is obtained from dc to $f = 598$ MHz (300 data points). Assume that only the first 100 time-data points (up to $t = 20.00$ ns) and the first 140 frequency-data points (up to 278 MHz) are available. In the time-domain data, the multiple reflections have been ignored, however, that information is available in the low-frequency data. Solving for the matrix equation (20) using the available data, the time-domain response is extrapolated to 300 points (up to $f = 598$ MHz). Given a time-bandwidth product of about 5.56, we extrapolate to a time-bandwidth product of 29.9.

$$\begin{bmatrix} h_0(t_1/q_1) & h_1(t_1/l_1) & \cdots & h_{N-1}(t_1/q_1) & h_{N-1}(t_1/q_1) \\ \vdots & \vdots & \vdots & \vdots & \vdots \\ h_0(t_{M_1}/q_1) & h_1(t_{M_1}/q_1) & \cdots & h_{N-2}(t_{M_1}/q_1) & h_{N-1}(t_{m_1}/q_1) \\ h_0(f_1/q_2) & 0 & \cdots & 0 & (-1)^{N/2-1} h_{N-1}(f_1/q_2) \\ \vdots & \vdots & \vdots & \vdots & \vdots \\ h_0(f_{M_2}/q_2) & 0 & \cdots & 0 & (-1)^{N/2-1} h_{N-1}(f_{M_2}/q_2) \\ 0 & -h_1(f_1/q_2) & \cdots & (-1)^{N/2-1} h_{N-1}(f_1/l_2) & 0 \\ \vdots & \vdots & \vdots & \vdots & \vdots \\ 0 & h_1(f_{M_2}/q_2) & \cdots & (-1)^{N/2} h_{N-2}(f_{M_2}/q_2) & 0 \end{bmatrix}_{(M_1+2M_2)\times N} \begin{bmatrix} a_1 \\ a_2 \\ \vdots \\ a_{N-1} \end{bmatrix}_{N\times 1}$$

$$= \begin{bmatrix} \sqrt{q_1}\, x(t_1) \\ \sqrt{q_1}\, x(t_{M_1}) \\ \sqrt{q_2}\, X_R(f_1) \\ \vdots \\ \sqrt{q_2}\, X_R(f_{M_2}) \\ \sqrt{q_2}\, X_I(f_1) \\ \vdots \\ \sqrt{q_2}\, X_I(f_{M_2}) \end{bmatrix}_{(M_1+2M_2)\times 1} \tag{20}$$

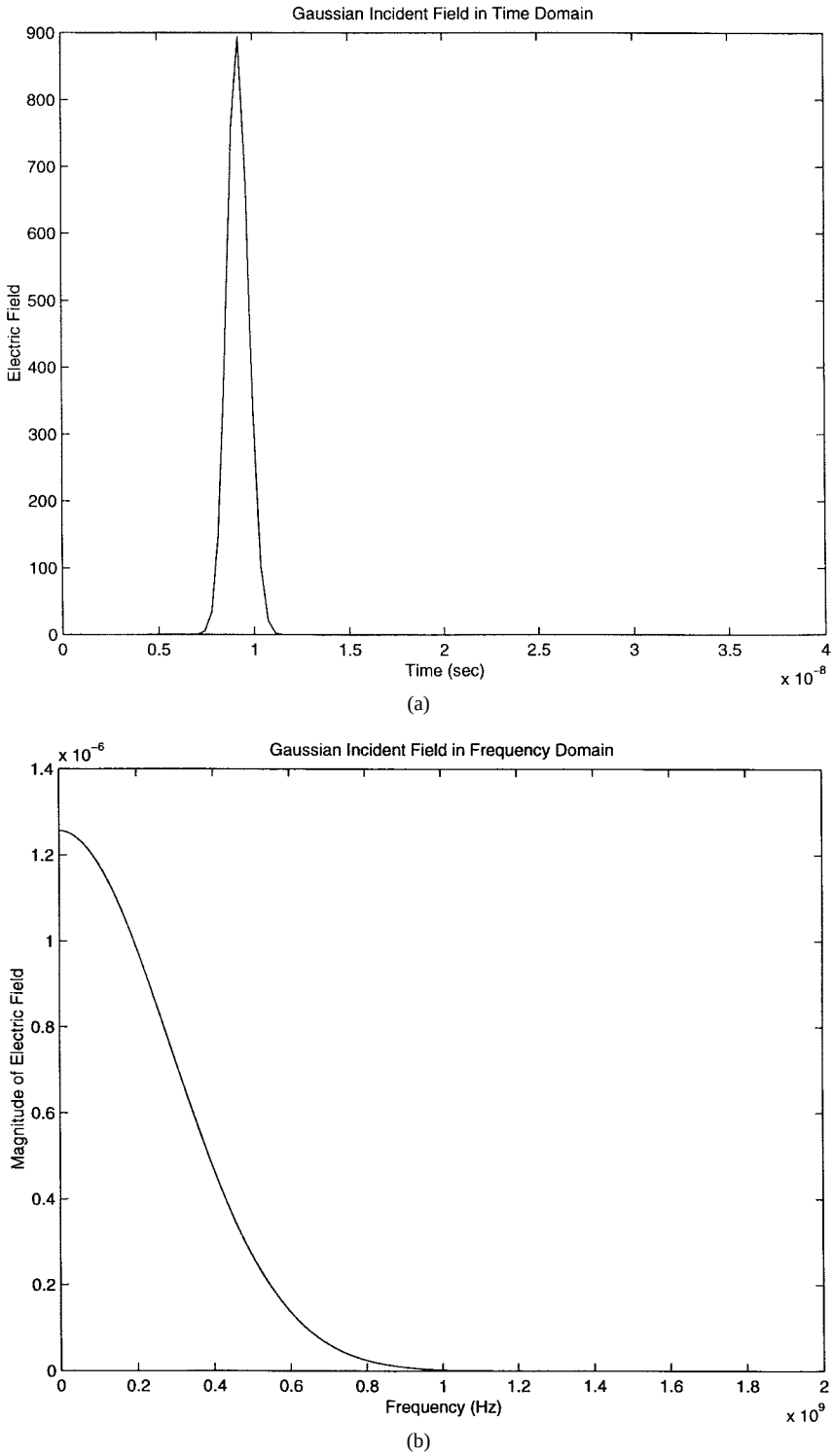

Fig. 1. (a) Time-domain representation of the Gaussian pulse. (b) Spectrum of the incident Gaussian pulse.

The order of expansion (N) is chosen to be 68 and the time-domain signal was centered about it second zeroth-crossing, i.e., $t_o = 10.23$ ns (denoted by "$*$" in the plots). A choice of q_2 was made such that the entire time axis (with the time shift) and the frequency axis were roughly mapped in the range $(-12,\ 12)$.

From Fig. 3, it can be seen that the time-domain reconstruction is almost indistinguishable from the actual (MOT) data. The origin of time axis in the AH expansion has been marked by an X. The reconstruction in the frequency domain is also very good, as can be seen from the real and imaginary parts of the frequency-domain data are given in Figs. 4 and 5. The y-axis marked $x(t)$ represents the current at that edge as a function of time and $X(f)$ is the value of the transfer function at a frequency f.

B. Example 2—Equal Plates

Two equal plates of side 1 m are placed as in the previous example, but the separation between the plates is reduced to

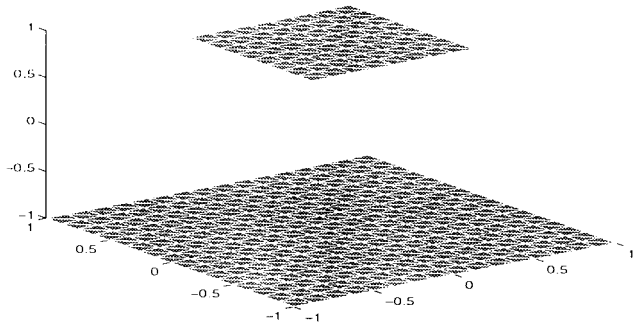

Fig. 2. Discretization of the two unequal plates.

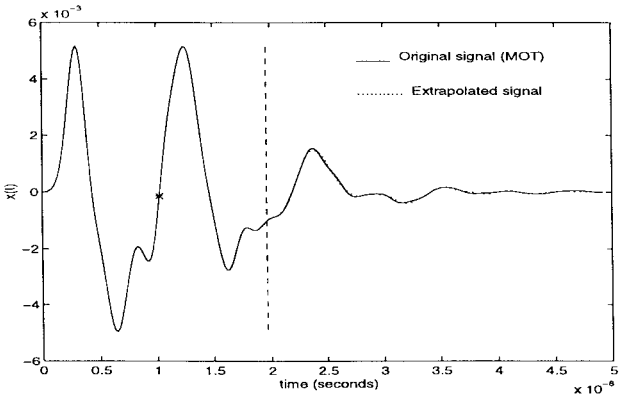

Fig. 3. Time-domain response at the smaller plate ($N = 68$).

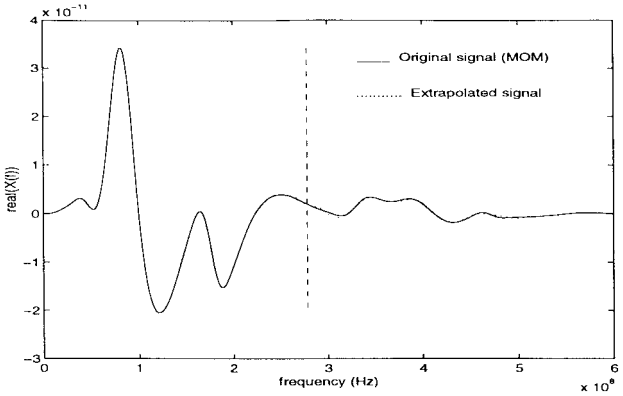

Fig. 4. Frequency-domain response at the smaller plate—real part ($N = 68$).

0.25 m so as to increase the resonance. The excitation arrives from $\theta = 0$, $\phi = 0$, i.e., along the negative z-direction. $\mathbf{u}_i$ is along the x-axis. Here, $\sigma = 0.59$ ns and $t_o = 2.30$ ns. The time step used is 160.1 ps. The edge under consideration is in the y-direction and close to the center of the upper plate.

In this example, the MOT algorithm is used to obtain time-domain response from $t = 0$ to $l = 124.8$ ns (780 data points). Also, the frequency-domain response is obtained using the MoM program from dc to $f = 898$ MHz (450 data points). Assume that only the first 120 time-data points (up to $l = 19.20$ ns) and the first 150 frequency-data points (up to $f = 298$ MHz) are available. Using this data, the time-domain response is extrapolated to 780 points (up to $l = 124.8$ ns) and the frequency-domain response is extrapolated to 450 points (up to $f = 898$ MHz). Given a time-bandwidth product of 5.72, we extrapolate to a time-bandwidth produce to 112.

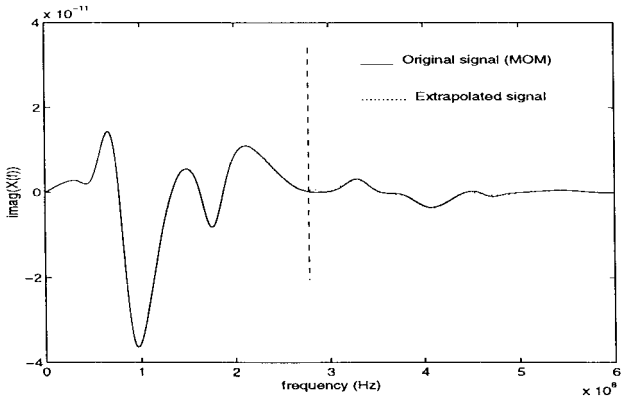

Fig. 5. Frequency-domain response at the smaller plate—imaginary part ($N = 68$).

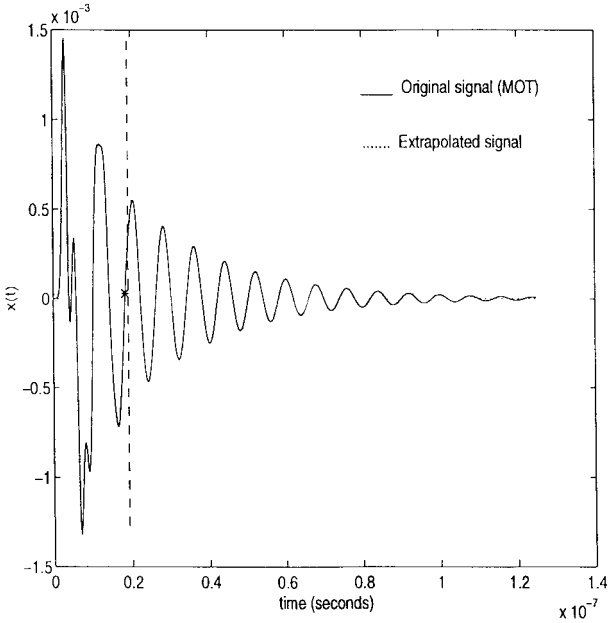

Fig. 6. Time-domain response at the upper plate ($N = 200$).

The order of expansion (N) was taken to be 200, and the time-domain signal was centered about its sixth zeroth-crossing, i.e., $t_o = 18.76$ ns. A choice of q_2 was made such that the entire response (shifted) t- and f-axes were sealed in the range $(-23, 23)$.

From Fig. 6, it can be seen that the time-domain reconstruction is almost identical to the actual (MOT) data. The origin of the AH expansion in the time domain has been marked by an X. The reconstruction in the frequency domain agrees closely with actual MoM data, as can be seen from Figs. 7 and 8. The point here is that there are multiple reflections that need to be taken into account in the time domain. However, by taking time-domain data only up to 19.20 ns, we are omitting the various reflections. If the complementary low-frequency information was not there, then it would not have been possible to extend the time-domain information.

C. Example 3—Plate Sphere

A plate–sphere combination is considered next, with the sphere of radius 1 m centered at the origin and separation of 5 m. The actual discretization is shown in Fig. 9. The

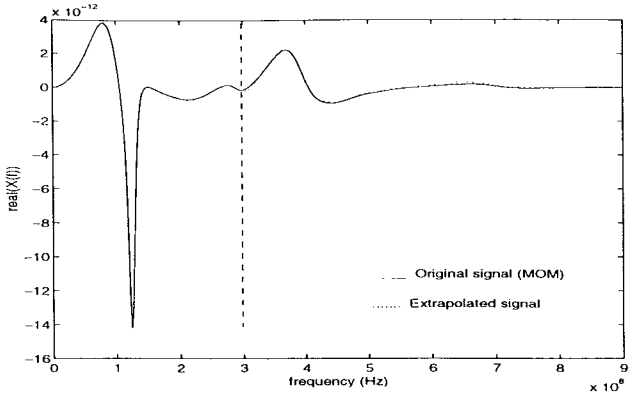

Fig. 7. Frequency-domain response at the upper plate—real part ($N = 200$).

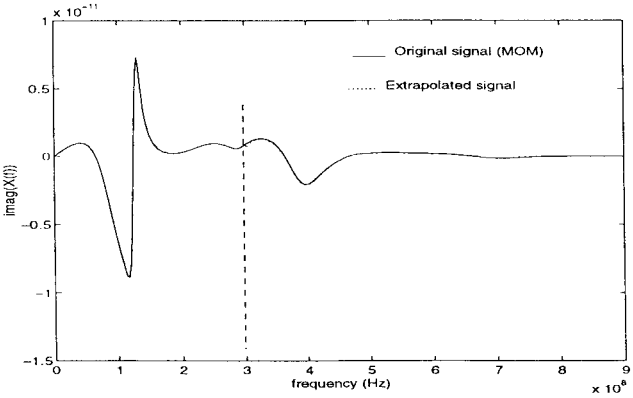

Fig. 8. Frequency-domain response at the upper plate—imaginary part ($N = 200$).

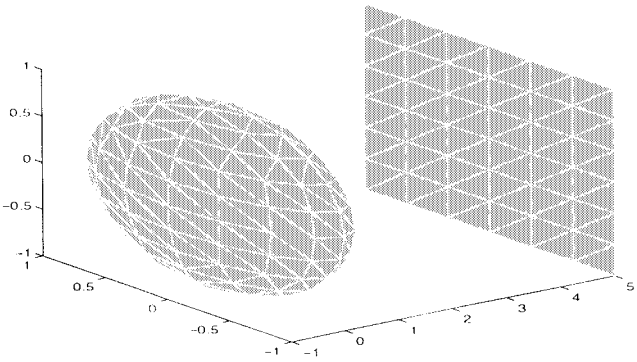

Fig. 9. Discretization of the plate–sphere structure.

excitation arrives along $\theta = \pi/2, \phi = 0$, i.e., along the negative x-direction, behind the plate. $\mathbf{u}_i$ is along the z-axis. In this example, $\sigma = 2.359$ ns and $t_o = 9.20$ ns. The time step used in the MOT program is 0.484 ns. The edge under consideration is on the plate, in the y-direction, and close to the center.

The time-domain response is obtained using the MOT algorithm from $t = 0$ to $l = 145$ ns (300 data points). Also, the frequency-domain response is obtained using the MoM program from dc to $f = 249$ MHz (250 data points). Using the first 80 time data points (up to $t = 38.67$ ns) and the first 80 frequency data points (up to $f = 79$ MHz), the time-domain response is extrapolated to 300 points (up to $t = 145$ ns) and

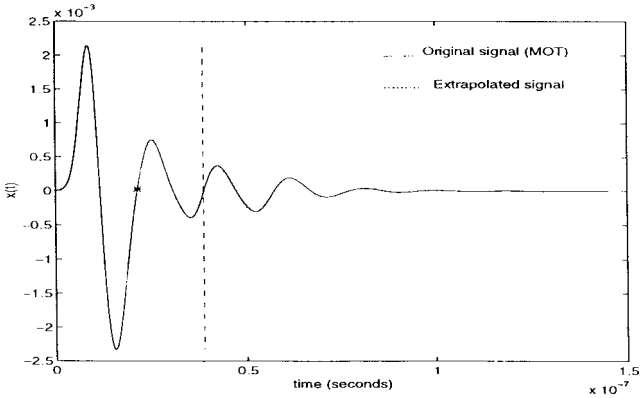

Fig. 10. Time-domain response at the plate ($N = 66$, 5-m separation).

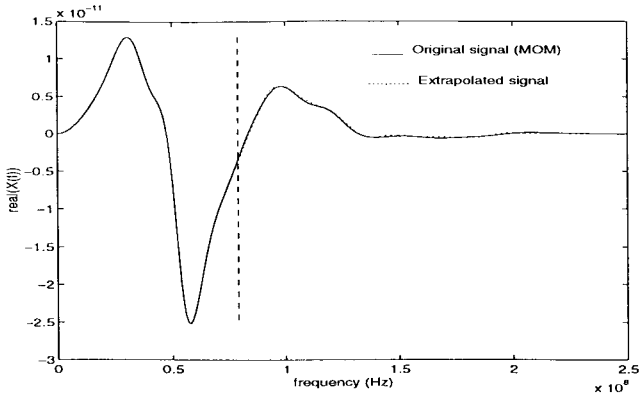

Fig. 11. Frequency-domain response at the plate—real part ($N = 66$, 5-m separation).

the frequency-domain response is extrapolated to 250 points (up to $f = 249$ MHz). In this example, given a time-bandwidth product of 3.05, we extrapolate to a time-bandwidth product of about 36.

The order the expansion (N) was chosen to be 66 and the time-domain signal is centered about its second zeroth-crossing, i.e., $t_o = 21.27$ ns. q_2 is chosen such that entire response (shifted) t- and f-axes are mapped in the range $(-11, 11)$.

The time-domain response reconstruction is agreeable to the actual MOT data, as seen in Fig. 10. The origin of the AH expansion in the time domain has been marked by an X. From Figs. 11 and 12, it can be seen that the frequency response also has reasonably good reconstruction using the AH expansions.

D. Separation of 12 m

The separation between the sphere and plate is increased to 12 m. All the other parameters are kept unchanged.

The time-domain response is obtained using the MOT algorithm from $t = 0$, $t = 145$ ns (300 data points). Also, the frequency-domain response is obtained using the MoM program from dc to $f = 249$ MHz (250 data points). Using the first 50 time data points (up to $t = 24.17$ ns) and the first 80 frequency data points (up to $f = 79$ MHz), the time-domain response is extrapolated to 300 points (up to $t = 45$ ns) and the frequency-domain response is extrapolated to 250 points

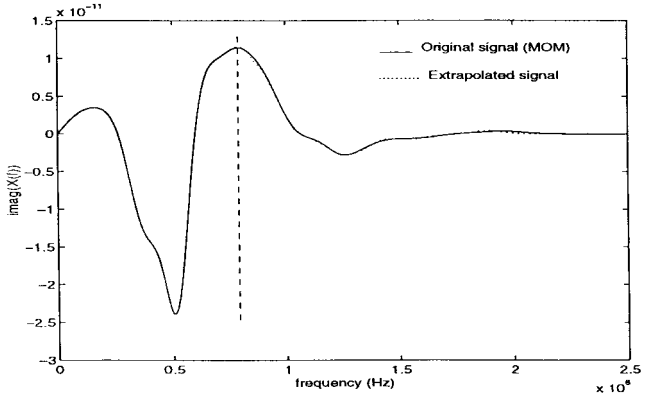

Fig. 12. Frequency-domain response at the plate—imaginary part ($N = 66$, 5-m separation).

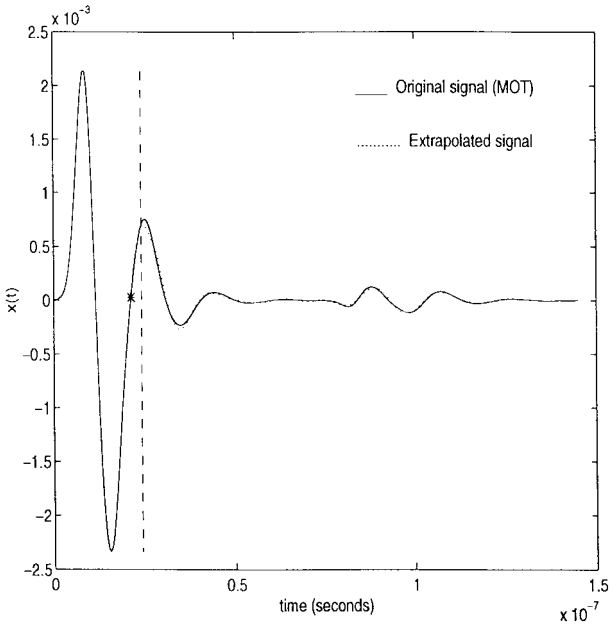

Fig. 13. Time-domain response at the plate ($N = 84$, 12-m separation).

(up to $f = 49$ MHz). In this example, given a time-bandwidth product of 1.91, we extrapolate to a time-bandwidth product of about 36.

It is important to point out that, in this time-domain data, there is no information about the sphere. This means that by taking only 50 data points in time, the incident pulse has crossed the plate, but did not arrive at the sphere. However, the information about the sphere is available in the low-frequency-domain results. Therefore, the information is complementary. By extrapolating or solving the problem in just one domain would not be sufficient to obtain the complete answer.

The order of the expansion (N) was chosen to be 84 and the time-domain signal is centered about its second zeroth-crossing, i.e., $t_o = 1.27$ ns. q_2 is chosen such that entire response (shifted) t- and f-axes are mapped in the range $(-12, 12)$.

The time-domain response reconstruction is agreeable to the actual MOT data, as seen in Fig. 13. As can be seen from Figs. 14 and 15, the frequency-domain response agrees reasonably well with the extrapolated response.

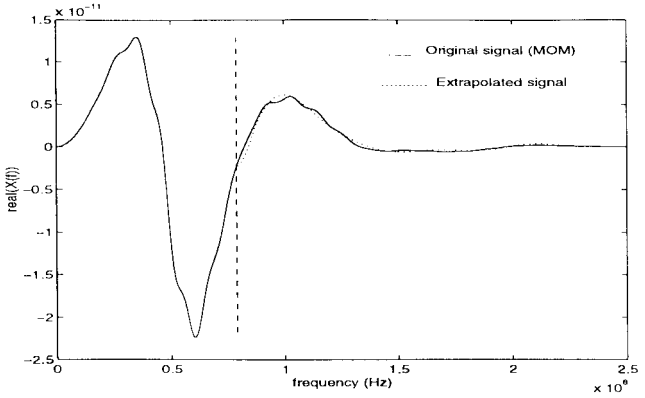

Fig. 14. Frequency-domain response at the plate—real part ($N = 84$, 12-m separation).

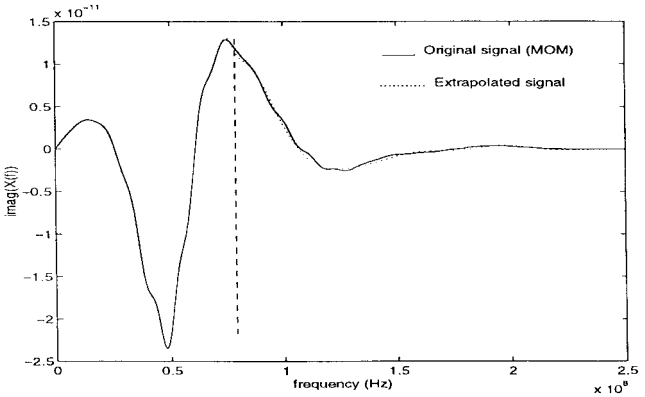

Fig. 15. Frequency-domain response at the plate—imaginary part ($N = 84$, 12-m separation).

E. Example 4—Cavity

In this example, a rectangular cavity of dimensions 1 m 1 m $\times$ 4 m, centered at the origin with its faces lined up along the three coordinate axes and its length along the x-axis. The face at $x = 4$ m is open. The excitation arrives from the direction $\theta = (5\pi/6)$, $\phi = (\pi/6)$, and $\mathbf{u}_i$ is along $\theta = (\pi/6)$, $\phi = (\pi/6)$. In this example, $\sigma = 1.18$ ns and $t_o = 4.56$ ns. The time step chosen for the MOT program is 0.267 ns. The edge under consideration is in the x-direction, close to the open end and at $z = 0.5$ m.

The time-domain response of an edge near the entrance to the cavity is calculated using the MOT algorithm from $t = 0$ to $t = 133.33$ ns (500 data points). Also, the frequency-domain response is calculated with the MoM program from dc to $f = 498$ MHz (250 data points). Assuming that only the first 100 t-data points (up to $t = 32$ ns) and the first 120 f-data points (up to $f = 198$ MHz), the time-domain response was extrapolated to 500 data points (up to $t = 133.33$ ns) and the frequency-domain response is extrapolated to 250 points (up to $f = 498$ MHz). Given a time bandwidth of 6.34, we extrapolate to a time-bandwidth product of about 66.

N was chosen to be 105 and the t-domain response was centered about its seventh zeroth-crossing, i.e., $t_o = 29.6$ ns. q_2 is chosen such that the entire response (shifted) t- and f-axes are mapped in the range $(-16, 16)$.

From Fig. 16, the time-domain response can be seen to closely agree with the actual MOT data. The frequency-domain

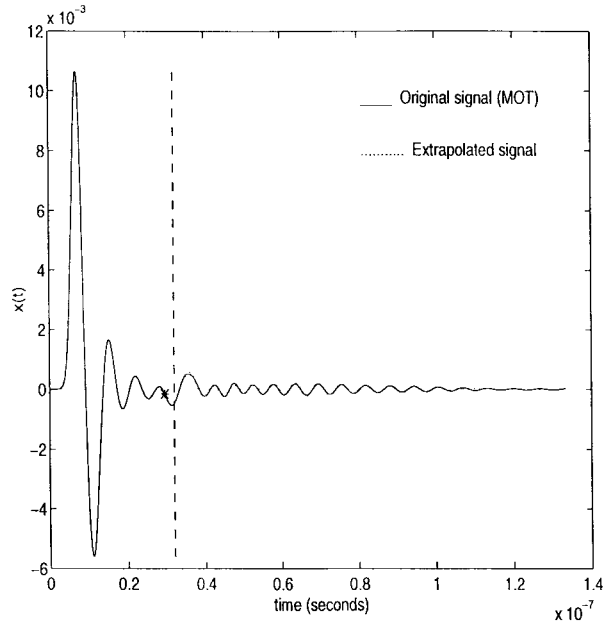

Fig. 16. Time-domain response of the cavity ($N = 105$).

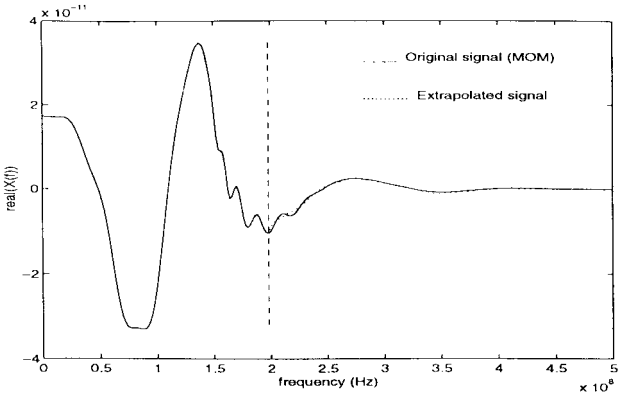

Fig. 17. Frequency-domain response of the cavity—real part ($N = 105$).

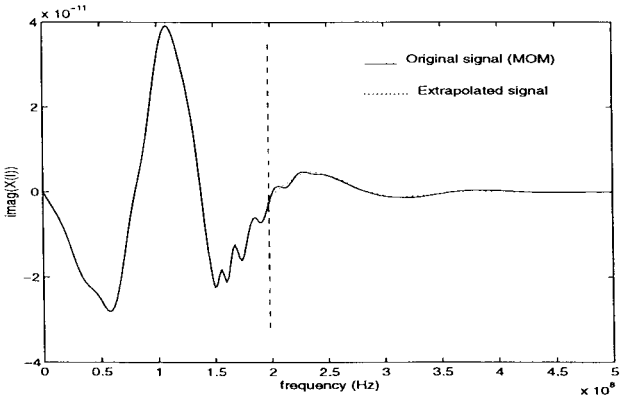

Fig. 18. Frequency-domain response of the cavity—imaginary part ($N = 105$).

reconstruction is agreeable in comparison to the actual MoM data, as can be seen from Figs. 17 and 18.

F. Example 5—Cone Hemisphere

In this example, we have a combination of a cone and hemisphere, with the hemisphere attached to the base of the cone and the axis along the z-direction. The base of the cone and hemisphere have a radius of 1 m, and the height of the cone is 4 m. Due to the instability of the EFIE time-domain formulation, in this example, the MFIE is used with quadrilateral patching [7].

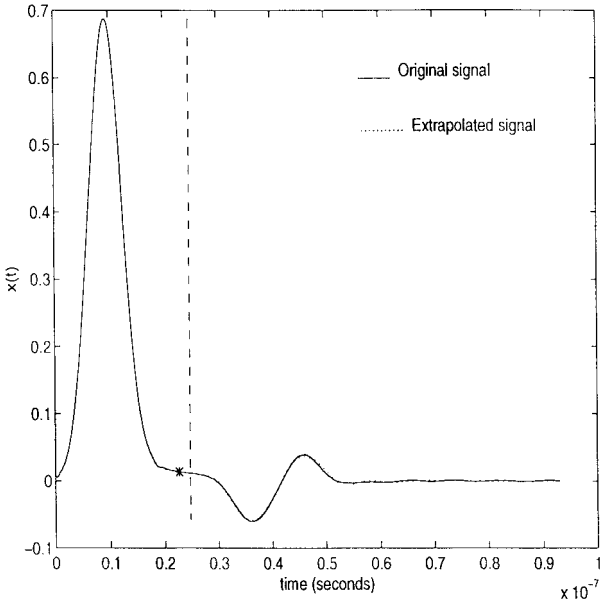

Fig. 19. Time-domain response of the cone hemisphere ($N = 28$).

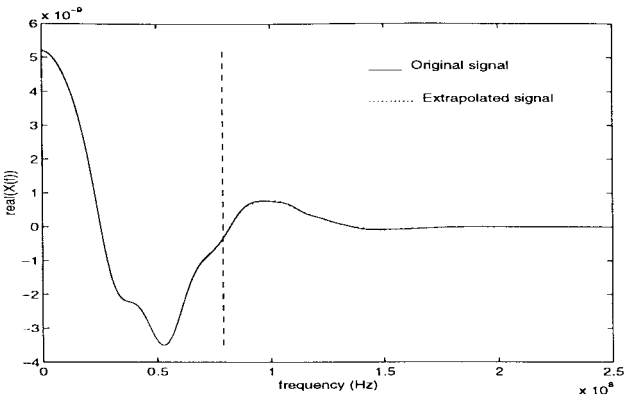

Fig. 20. Frequency-domain response of the cone hemisphere—real part ($N = 28$).

The excitation arrives from $\theta = 0$, $\phi = 0$, i.e., along the negative z-direction. $\mathbf{u}_i$ along the y-axis. In this example, $\sigma = 2.948$ ns and $t_o = 11.495$ ns. The time step used is 206.67 ps and the frequency step is 1 MHz. The edge under consideration is close to the vertex of the cone.

The time-domain response is calculated using the MOT program from $t = 0$ to $t = 93$ ns (450 points). Also, the frequency-domain response is calculated using the MoM algorithm from dc to $f = 249$ MHz (250 data points). Using the first 120 t-data up to $t = 24.8$ ns and the first 80 f-data points (up to $f = 79$ MHz), the time-domain response is extrapolated to 450 data points (up to $t = 93$ ns) and the frequency-domain response is obtained up to 250 points (up to $f = 249$ MHz). In this example, starting with a time-bandwidth product of 1.96, we extrapolate to a time-bandwidth

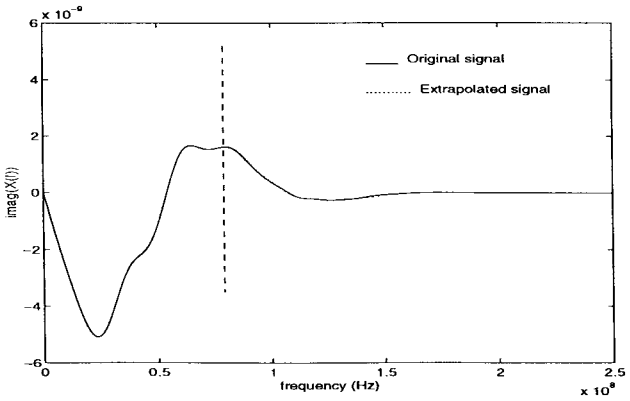

Fig. 21. Frequency-domain response of the cone hemisphere—imaginary part ($N = 28$).

product of about 23 (considering the finite support of the signals).

N was chosen to be 28 and the time-domain response was centered about its first zeroth-crossing, i.e., $t_o = 22.73$ ns. And q_2 is chosen such that the entire response (shifted) t- and f-axes are scaled in the region of $(-7, 7)$.

From Fig. 19, the extrapolated time-domain response is agreeable with the MOT data. The frequency-domain responses agree reasonably well with the actual MoM data, as can be seen from Figs. 20 and 21.

V. Conclusion

In this paper, we have applied the AH polynomials to the problem of extrapolating at a spatial location that is excited by an incident wave. Six examples have been considered—parallel-plate resonators (equal and unequal size plates), plate–sphere combination with two different separations, resonating cavity, and a cone–hemisphere combination. Using early time and low-frequency data, we have demonstrated good extrapolation in both domains can be obtained even though a large amount of information is missing in one domain. The information at early time and low frequency is complementary. It is important to point out that, in this methodology, we are not creating any new information, but only processing it in an efficient manner to obtain the complete response.

References

[1] R. S. Adve, T. K. Sarkar, Q. M. Pereira-Filho, and S. M. Rao, "Extrapolation of time-domain responses from three dimensional conducting objects utilizing the matrix pencil techniques," *IEEE Trans. Antennas Propagat.*, vol. 45, pp. 147–156, Jan. 1997.

[2] R. S. Adve, T. K. Sarkar, S. M. Rao, E. K. Miller, and D. R. Pflug, "Application of the Cauchy method for extrapolating/interpolating narrow-band system responses," *IEEE Trans. Microwave Theory Tech.*, vol. 45, pp. 837–845, May 1997.

[3] R. S. Adve and T. K. Sarkar, "Simultaneous time and frequency-domain extrapolation," *IEEE Trans. Antennas Propagat.*, vol. 46, pp. 484–493, Apr. 1998.

[4] S. Narayana, T. K. Sarkar, and R. S. Adve, "A comparison of 2 techniques for the interpolation/extrapolation of frequency domain responses," *Digital Signal Processing*, vol. 6, no. 1, pp. 51–67, Jan. 1996.

[5] S. M. Rao, "Electromagnetic scattering and radiation of arbitrarily shaped surfaces by triangular patch modeling," Ph.D. dissertation, Dept. Elect. Eng., Univ. Mississippi, University, MS, 1978.

[6] D. A. Vechniski, "Direct time-domain analysis of arbitrarily shaped conducting or dielectric structures using patch modeling techniques," Ph.D. dissertation, Dept. Elect. Eng., Auburn Univ., Auburn, AL, 1992.

[7] D. A. Vechniski, S. M. Rao, and T. K. Sarkar, "Transient scattering from three-dimensional arbitrarily shaped dielectric bodies," *J. Opt. Soc. Amer. A, Opt. Image Sci.*, vol. 11, no. 4, Apr. 1994.

[8] G. H. Golub and C. F. Van Loan, *Matrix Computations.* Baltimore, MD: The Johns Hopkins Press, 1991.

Murli Mohan Rao received the B.Tech. degree in electronics and communication engineering from the Indian Institute of Technology, Madras, India, in 1994, and the M.S. degree in electrical engineering from Syracuse University, Syracuse, NY, in 1997.

From 1994 to 1995, he was with Infosys Technologies, Bangalore, India. In 1997, he was with Ariel Corporation, as a Digital Signal Processing Engineer. He is currently with rlemedia, Bell Laboratories, Lucent Technologies, Holmdel, NJ. His research interests are in the areas of signal processing as applied to numerical electromagnetics, communication theory, and wireless communications. His professional interests are in fast analog modems, and he is currently involved with the digital subscriber line (DSL) broad-band modem.

Tapan Kumar Sarkar (S'69–M'76–SM'81–F'92) received the B.Tech. degree from the Indian Institute of Technology, Kharagpur, India, in 1969, the M.Sc.E. degree from the University of New Brunswick, Fredericton, N.B., Canada, in 1971, and the M.S. and Ph.D. degrees from Syracuse University, Syracuse, NY, in 1975.

From 1975 to 1976, he was with the TACO Division, General Instruments Corporation. From 1976 to 1985, he was with the Rochester Institute of Technology, Rochester, NY. From 1977 to 1978, he was a Research Fellow at the Gordon McKay Laboratory, Harvard University, Cambridge, MA. He is currently a Professor in the Department of Electrical and Computer Engineering, Syracuse University, Syracuse, NY. His current research interests involve numerical solutions of operator equations arising in electromagnetics and signal processing with application to system design. He has authored or co-authored over 210 journal articles and numerous conference papers and has written chapters in ten books, including *Iterative and Self Adaptive Finite-Elements in Electromagnetic Modeling* (Norwood, MA: Artech House, 1998). He was appointed U.S. research council representative to many URSI General Assemblies. He was the chairman of the Intercommission Working Group of International URSI General Assemblies. He was the chairman of the Intercommission Working Group of International URSI on Time-Domain Metrology (1990–1996). He is on the Editorial Board of the *Journal of Electromagnetic Waves and Applications*.

Dr. Sarkar is a member of Sigma Xi and the International Union of Radio Science Commissions A and B. He is a registered Professional Engineer in the state of New York. He received the Best Paper Award presented by the IEEE Transactions on Electromagnetic Compatibility in 1979 at the 1997 National Radar Conference. He was an associate editor for feature articles of the IEEE Antennas and Propagation Society International Symposium and URSI Radio Science Meeting. He received the title "Docteur Honoris Causa" from the Universite Blaise Pascal, Clermon Ferrand, France in 1998. He received one of the Best Solution Awards presented at the Rome Air Development Center (RADC) Spectral Estimation Workshop in May 1977.

Raviraj S. Adve, photograph and biography not available at the time of publication.

Tricha Anjali was born in Hardwar, India. She received the Integrated M.Tech. degree in electrical engineering from the Indian Institute of Technology, Bombay, India, in 1998 and is currently working toward the Ph.D. degree in electrical engineering at Syracuse University, Syracuse, NY.

Her research interests include signal processing and its application in numerical electromagnetics.

Jesús Fornieles Callejón was born in El Ejido, Almería, Spain, in 1967. He received the B.Sc., M.Sc., and Ph.D. (*cum laude*) degrees from the University of Granada, Spain, in 1990, 1992, and 1994, respectively, all in physics.

From 1992 to 1999, he was an Assistant Professor and, in 1999, he was appointed Associate Professor at the University of Granada, Granada, Spain. He has been a Visiting Scholar in EPFL, Lausanne, Switzerland, Syracuse University, Syracuse, NY, University of Dundee, Dundee, Scotland, and Imperial College, London, U.K. His current research interest is the development of numerical and analytical methods for solving transient electromagnetic problems. He was the recipient of a grant that allowed him to work with the Electromagnetic Research Group, University of Granada (1990–1992).